

MAGNETIC MEASUREMENTS AND KINETIC ENERGY OF THE SUPERCONDUCTING CONDENSATE IN $\text{SmBa}_2\text{Cu}_3\text{O}_{7-\delta}$

J.P. Peña^{1,2}, D.B. Martínez¹, C.A. Parra Vargas¹, A.G. Cunha³,
J.L. Pimentel Jr.², P. Pureur²

July 2, 2018

¹ Grupo de Física de Materiales, Universidad Pedagógica y Tecnológica de Colombia, Av. Central del Norte, Tunja, Colombia.

² Instituto de Física, Universidade Federal do Rio Grande do Sul, Av. Bento Gonçalves 9500, C.P. 15051, 91501-970, Porto Alegre, RS, Brazil.

³ Departamento de Física, Universidade Federal do Espírito Santo, Av. Fernando Ferrari 514, Campus Goiabeiras, 29075-910, Vitória, ES, Brazil.

Abstract

We report in-field kinetic energy results in the temperature region closely below the transition temperature of two differently prepared polycrystalline samples of the superconducting cuprate $\text{SmBa}_2\text{Cu}_3\text{O}_{7-\delta}$. The kinetic energy was determined from magnetization measurements performed above the irreversibility line defined by the splitting between the curves obtained according the ZFC and FC prescriptions. The results are analyzed in the intermediate field regime where the London approximation can be used for describing the magnetization. From the analysis, estimations were carried out for the penetration depth and the upper critical field of the studied samples. The difference between the kinetic energy magnitudes for the two studied samples is ascribed to effects from granularity.

Key words: kinetic energy density, vortex lattice, granularity.

1 Introduction

The experimental study of the kinetic energy of the charge carriers in the high temperature cuprate superconductors (HTCS) become an important subject in

view of the new theoretical approaches predicting that, in the absence of an applied magnetic field, pairing in these materials results from a decrease of the kinetic energy term upon condensation [1,2]. This prediction is opposite to that of the BCS theory, where the kinetic energy of the carriers increases when the system enters the superconducting state [3]. Experimentally, the situation is less clear because of the relatively small change of the kinetic energy in the condensate with respect to that of the normal state. Optical conductivity measurements in optimally doped and underdoped $\text{Bi}_2\text{Sr}_2\text{CaCu}_2\text{O}_{8+d}$ (Bi-2212) suggests that the observed spectral weight transfer that occurs below the superconducting transition is in agreement with the unconventional scenario of decreasing kinetic energy [4]. On the other hand, when this cuprate is slightly overdoped, results are rather in accordance with the BCS predictions [5].

A simpler situation occurs in a type II superconductor when a magnetic field is applied. In that case, it is expected that the kinetic energy of the condensate always increase because of the flux expulsion and vortex formation [6]. Useful informations may be obtained on the order parameter and other basic properties of type II superconductors from studies of this energy term [7]. In the case discussed here, we are interested in the kinetic energy associated to the currents around the vortices generated by the action of an applied external magnetic field.

Theoretically, it was demonstrated from applying the virial theorem in the framework of the Ginzburg-Landau (G-L) theory [8] that the average kinetic energy density of a large κ superconductor may be written as [6,7]

$$E_K = -\vec{M} \cdot \vec{B}, \quad (1)$$

where \vec{M} is the equilibrium magnetization and \vec{B} is the magnetic induction. Inside a superconducting sample, the induction (in the SI system) may be written as $\vec{B} = \mu_0\vec{H} + \mu_0(1 + \eta)\vec{M}$, where μ_0 is the vacuum permeability, \vec{H} is the applied field and η is the sample dependent geometric factor related to the dipolar field. Then, for obtaining the kinetic energy density from magnetization measurements, it is useful to re-write equation (1) as

$$E_K = -\mu_0\vec{M} \cdot \vec{H} - \mu_0(1 + \eta) M^2. \quad (2)$$

The in-field kinetic energy density was determined for some low and high T_c superconductors in the references [6],[9] and [10]. The results reported for Nb [9] and for a Pb-In alloy [10] are in agreement with the expectations derived from the Abrikosov treatment of the G-L theory, as well as with general BCS predictions. On the other hand, in cuprates as optimally doped and underdoped $\text{YBa}_2\text{Cu}_3\text{O}_x$ (YBCO) [9], optimally doped Bi-2212 [9] and $\text{La}_{1.9}\text{Sr}_{0.1}\text{CuO}_4$ [10] an appreciable amount of the in-field kinetic energy subsists up to temperatures well beyond T_c . Authors in references [9] and [10] identify this behavior to a pseudogap effect, although the influence of strong thermal fluctuations cannot be ruled out as an alternative explanation.

In order to study the differences induced by the microscopic morphology in the kinetic energy, here we report magnetization measurements and in-field

kinetic energy density estimations in two different polycrystalline samples of $\text{SmBa}_2\text{Cu}_3\text{O}_{7-\delta}$ (Sm-123). The experiments were performed in several applied fields. However, the extraction of $E_K(T, H)$ is restricted to the temperature range near T_c , where the equilibrium magnetization can be unambiguously obtained from coincident and reproducible ZFC and FC measurements. Results are compared to those obtained in YBCO and Bi-2212 single crystals [9,10]. The magnitude of the kinetic energy of our polycrystalline samples is considerably smaller than that of single crystal samples.

2 Experimental

Two samples of polycrystalline $\text{SmBa}_2\text{Cu}_3\text{O}_{7-\delta}$ (Sm-123) were independently produced using the solid state reaction method. The employed procedures are described below. The precursor compounds Sm_2O_3 (purity 99.99%), BaCO_3 (purity 99.8%) and CuO (purity 99.995%) were used for the preparation of the samples. For the sample labeled as Sm-I, the precursors were mixed and macerated during two hours in an agate mortar, pressed at 3 tons into a cylindrical shape and submitted to a calcination process at 850°C during 15 hours. After furnace cooling to room temperature, the resulting pellet was finely powdered again, pressed and subjected to two sintering processes at 870°C and 890°C for 45 hours each one. The cylindrical sample was then oxygenated by exposure to an oxygen atmosphere while decreasing the temperature in the range $750\text{-}250^\circ\text{C}$ at rate of 12.5°C/h , then it was furnace cooled to room temperature. The preparation of sample Sm-II was also done in three steps but using different equipments and thermal processes. In the calcination process, the macerated and pressed precursors were heated up to 850°C and kept at this temperature during 48 hours. For the sintering step, the sample was heated up to 900°C at 150°C/h , kept at this temperature for 0.1 h, then heated up to 1040°C at 60°C/h . A 24 hours annealing was carried out at this temperature before cooling the sample at -60°C/h to 900°C where it was maintained for 0.1 h. Subsequently, the sample was cooled down to room temperature at 150°C/h . In the final oxygenation process, the sample Sm-II was heated again to 500°C and kept at this temperature during 0.1 h. Then, it was cooled to 350°C and kept at this temperature for 3 days. After that time, the sample was furnace cooled to room temperature.

Electrical resistivity measurements were performed in both samples. Transition temperatures determined from the maximum of the temperature derivative of the resistivity are $T_c = 92.7$ K for sample Sm-I and $T_c = 89.9$ K for sample Sm-II. The width of the resistive transition is around 3 K for both samples.

Zero field cooling (ZFC) and field cooling (FC) magnetization measurements in several applied fields ranging from 1 mT up to 5 T were performed using a XL5-MPMS SQUID magnetometer manufactured by Quantum Design Inc. Results were corrected for the demagnetization effects. The geometrical factors were estimated by approximating the samples's shape to an ellipsoid and making use of the calculations in reference [11]. The porosity of the ceramic samples

was also taken into account by comparing their measured densities and the theoretically expected value.

3 Results

3.1 Reversible Magnetization and Fluctuation Effects

Figure 1 shows representative magnetization versus temperature results in a temperature range encompassing the superconducting transition for the two studied samples. Panel (a) shows results for sample Sm-I and in panel (b) are plotted data for sample Sm-II. Experiments were performed according the ZFC and FC prescriptions. The irreversibility temperature T_{irr} denotes the point below which the pinning effects become important. We carried out our analyses in the temperature regime above T_{irr} , where the experimental data describe the equilibrium magnetization without ambiguity. The extension of the magnetically reversible regime in high applied fields is smaller for the sample Sm-II than for the sample Sm-I.

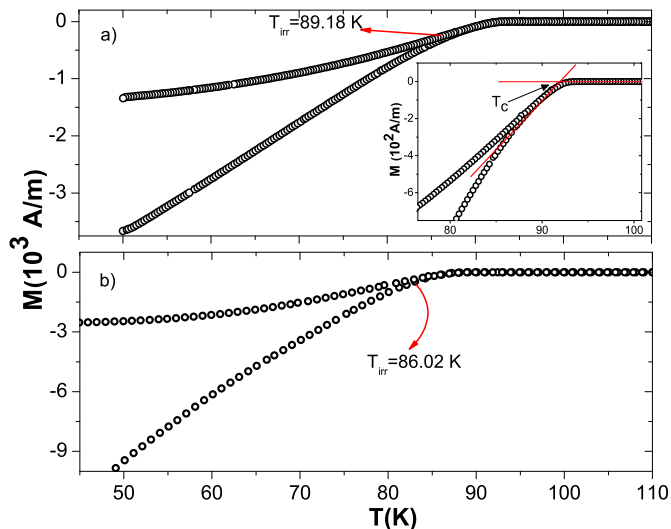


Figure 1: Zero field cooled (ZFC) and field cooled (FC) magnetization as functions of the temperature for polycrystalline $\text{SmBa}_2\text{Cu}_3\text{O}_{7-\delta}$ (Sm-123) measured at $\mu_0 H = 0.05$ T. Panel (a) shows results for sample Sm-I (see text), the inset illustrates the criterion used to define the in-field critical temperatures. Panel (b) shows results for sample Sm-II. The irreversibility temperature T_{irr} is signaled and denotes the splitting of the ZFC and FC curves. Corrections for the demagnetizing field effects are taken into account.

Figures 2(a) and 2(b) collect the characteristic temperatures T_c and T_{irr} in the presence of several applied fields for samples Sm-I and Sm-II, respec-

tively. The area delimited between the curves $T_c(H)$ and $T_{irr}(H)$ defines the reversible region where effects of the pinning energy are negligible. The field-dependent critical temperatures are determined by the intersection between the linearly extrapolated magnetizations in the normal and superconducting phases, as illustrated in the inset of Fig. 1(a). The irreversibility temperatures are determined by subtracting the ZFC magnetization from the FC one and applying the criterion used in reference [12]: the temperature where the difference $M_{FC}(T, H) - M_{ZFC}(T, H)$ deviates from the zero baseline defined by the high temperature data is assigned to $T_{irr}(H)$.

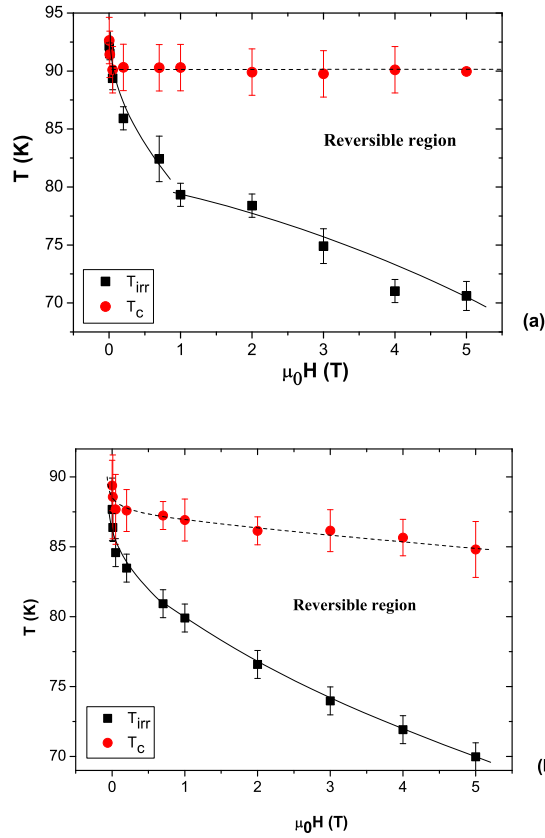


Figure 2: Critical temperatures and irreversibility temperatures as functions of the applied field for the samples Sm-I (a) e Sm-II (b). The continuous and dashed lines are guides for the eye.

The observed behaviour of $T_{irr}(H)$ on the two samples is typical of polycrystalline samples of HTCS [13] and mimics the observations in spin glass systems. For the sample Sm-I, in the low field and high temperature limit, the irreversibility temperatures decrease as a function of the applied field as

$[T_{irr}(0) - T_{irr}(H)] \sim H^{2/3}$, in analogy to the de Almeida-Thouless line [14]. As shown in Fig. 2(a), near $\mu_0 H = 0.5$ T, a crossover is observed in $T_{irr}(H)$ to a field dependence with inverse curvature that may be approximately fitted to a Gabay-Toulouse-like line [15] given by $[T_{irr}(0) - T_{irr}(H)] \sim H^2$. The behaviour observed in Fig. 2(a) was interpreted as the vortex glass analog of the crossover from the high-field Gabay-Toulouse transition to the low field de Almeida-Thouless instability observed in Heisenberg vector spin glasses [16]. As shown by Fig. 2(b) for sample Sm-II, a de Almeida-Thouless-like line describes the irreversibility line in the whole field range in this case. The results in Fig. 2 suggest that the effects from granularity are stronger in sample Sm-I.

3.2 Kinetic Energy

We assume that the G-L theory describes the equilibrium magnetization adequately in most of the reversible superconducting regime of our samples. Then, using the recipe of Doria et al. [6], in Figs. 3 (a) and (b) we plot the field induced kinetic energy given by equation (2) as a function of temperature for samples Sm-I and Sm-II, respectively. Results for magnetic fields ranging from 0.2 T up to 5 T are shown and the data are restricted to the temperature regime where the magnetization is reversible. The applied field range in our investigation enlarges significantly the regime studied in Ref. [9] for YBCO. Here, the kinetic energy density approaches linearly to the temperature axis and vanishes for $T \approx T_c(H)$. We do not observe a significant kinetic energy contribution above T_c , contrasting with the findings reported in Ref. [9]. On the other hand, E_K in Sm-123 and YBCO are qualitatively similar in the field and temperature range where the comparison is possible, even though results in YBCO were obtained for fields applied perpendicular to the Cu-O₂ atomic layers of a single crystal sample [9].

Although the similar field and temperature behavior shown by results for samples Sm-I and Sm-II in Fig. 3, these data differ quantitatively. For a given field and temperature, E_K is significantly larger for sample Sm-II. We attribute this difference to polycrystallinity. Indeed, the different routes employed to prepare our samples likely lead to distinct granular microstructures and granularity is known to underly the magnetic behavior of polycrystalline samples of the HTCS.

In the intermediate field regime, $H_{c1} \ll H \ll H_{c2}$, the interaction among the vortices is weak [3]. In this field region, the Cooper pair density may be considered uniform inside the sample excepting the vortex positions. In the case of extreme type II superconductors ($\kappa \gg 1$) as the HTCS, the variation of the order parameter in the vortex positions may be described by delta functions. Under such conditions the magnetization can be calculated with the London approximation to the G-L theory. In this case, the magnetization in SI units is [17]:

$$M(H) = -\frac{\phi_0}{8\mu_0\pi\lambda^2} \ln\left(\frac{\beta_L H_{c2}}{H}\right), \quad (3)$$

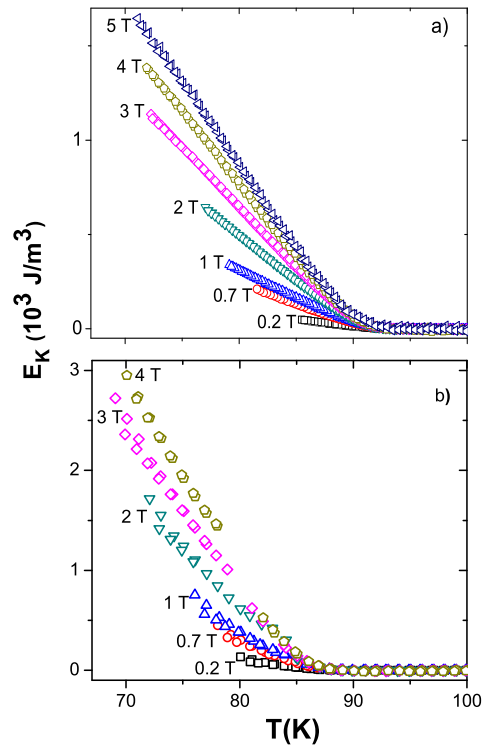


Figure 3: Kinetic energy density as a function of the temperature for samples (a) Sm-I and (b) Sm-II in the quoted applied fields.

where ϕ_0 is the quantum magnetic flux, μ_0 is the vacuum permeability, λ is the penetration length and β_L is a constant of order unity.

The substitution of the magnetization given by equation (3) in equation (2) yields:

$$\frac{E_K(\mu_0 H)}{\mu_0 H} = \frac{\phi_0}{8\pi\lambda^2\mu_0} \ln \frac{\beta_L\mu_0 H_{c2}}{\mu_0 H} - \left(\frac{\phi_0}{8\pi\lambda^2}\right)^2 \frac{1}{\mu_0^2 H} \left(\ln \frac{\beta_L\mu_0 H_{c2}}{\mu_0 H}\right)^2. \quad (4)$$

Fittings of the experimental data to equation (4) are displayed in Fig. 4 for samples Sm-I and Sm-II. From these fittings we estimate the penetration lengths and the upper critical field in the studied field and temperature ranges. The values obtained for $\lambda(T)$ and $H_{c2}(T)$ were corrected according the Hao and Clem model [18] and are shown in figs. 5 and 6, respectively.

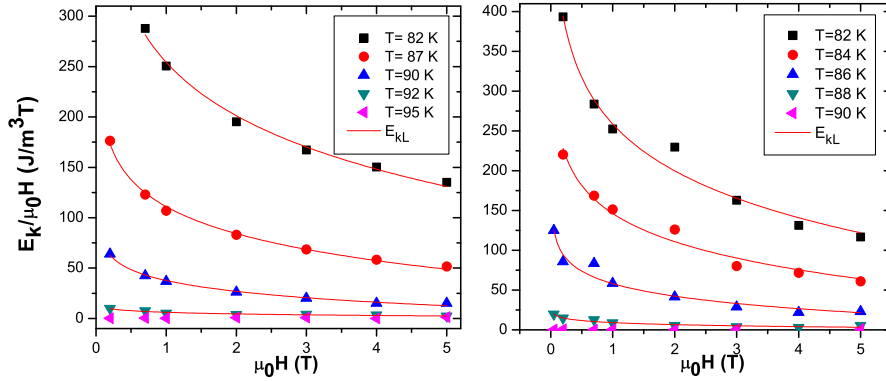


Figure 4: Kinetic energy per unit of field for the samples Sm-I (left) and Sm-II (right). The solid lines are fits of eq. (4) to the experimental data.

According to the mean-field theory, $\lambda(T) = \frac{1}{\sqrt{2}}\lambda(0)t^{-1/2}$ and $B_{c2}(T) = 1,83B_{c2}(0)t$ where $t = \frac{T_c - T}{T_c}$ is the reduced temperature [19]. In fig. 5, the values for $\lambda(T)$ for samples Sm-I and Sm-II are plotted as functions of $1/\sqrt{t}$. The fitted straight lines allow us to estimate $\lambda(0) = 516 \pm 12$ nm for sample Sm-I and $\lambda(0) = 363 \pm 7$ nm for sample Sm-II. These values are within the expected range, since the estimated penetration lengths are polycrystalline averages enhanced by granularity effects [20]. The larger $\lambda(0)$ found in sample Sm-I also suggests that the influence of granularity is stronger in this sample.

In fig. 6, the estimations for H_{c2} extracted from fittings in fig.4 are plotted as a function of the reduced temperature. Data for both samples align to a single straight line. From the slope of line we deduce that $B_{c2}(0) = 130$ T for Sm-123. This estimation is in good agreement with previous determinations of polycrystalline averages of the upper critical induced field in Y-123-type superconductors [19].

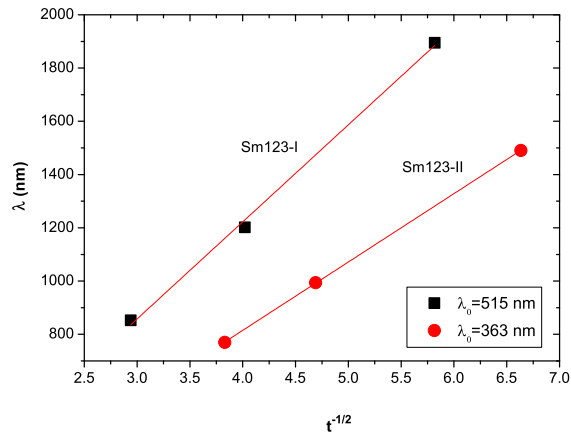


Figure 5: Penetration lengths for samples Sm-I and Sm-II deduced from fits of the data in fig. 4 to equation (4). Plots are made as functions of $1/\sqrt{t}$.

Since granularity leads the polycrystalline HTCS systems to behave as a superconducting glassy medium [21], the in-field kinetic energy in our Sm-123 samples may not be entirely accounted by the London approximation to the Ginzburg-Landau theory. So, one might consider that a complete description of the kinetic energy in granular HTCS should include the contributions of Josephson vortices [22] and intergrain chiralities [23]. However, as a first approximation, equation (4) furnishes a fairly good description of the data, showing that the intragrain vortices are indeed the dominant contribution to the condensate kinetic energy in Sm-123 in the investigated field-temperature range.

4 Conclusions

We studied experimentally the reversible magnetization and the field-induced kinetic energy density in two polycrystalline samples of the $\text{SmBa}_2\text{Cu}_3\text{O}_{7-\delta}$ cuprate superconductor. Analysis were restricted to the temperature range nearly below T_c , where the ZFC and FC magnetization are coincident. Fields up to 5 T were applied.

The theory proposed by M. Doria and co-workers [6,7] which is based on the application of the virial theorem to the Ginzburg-Landau free energy was used to describe the kinetic energy density in our samples. The magnitude of the kinetic energy was found larger for sample Sm-II than for sample Sm-I. We attributed this difference to the enhanced granularity effects in sample Sm-I. The identified contribution to the kinetic energy in both samples were attributed to intragrain vortices. Results could be interpreted by assuming the validity of London approximation to the Ginzburg-Landau theory. The penetration length and the upper critical field were calculated for both samples. The obtained

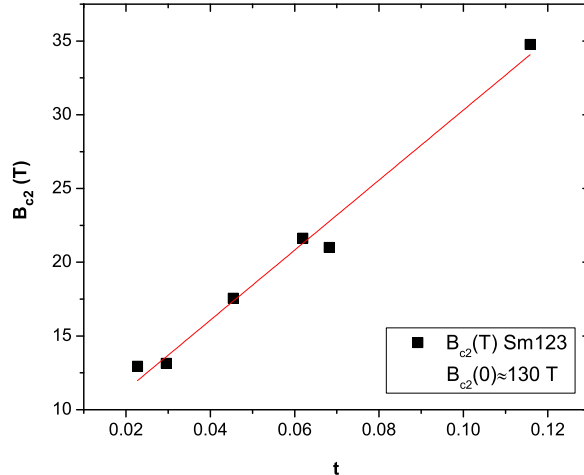


Figure 6: Upper critical field for samples Sm-I and Sm-II as deduced from the results in fig. 4. Data points are plotted as a function of the reduced temperature. A single straight line fits the data for both samples.

values are similar to those found in previous studies. The penetration length estimations corroborate the enhanced effects of granularity in sample Sm-I.

As a final conclusion, our results and analysis showed that the study of the in-field kinetic energy may improve the usual description of the magnetic response of superconductors based solely on magnetization results in the temperature range approaching T_c , where the pinning effects are inexistent.

Acknowledgments We thank Dr. Mauro Doria for enlightening discussions on the in-field kinetic energy of a superconducting condensate. This work was partially financed by the Brazilian agencies FAPERGS and CNPq under the grant PRONEX 10/0009-2.

References

- [1] V.J. Emery and G. Reiter, Phys. Rev. B 38, 4547 (1988).
- [2] J.E. Hirsch, Physica C 201, 347 (1992).
- [3] M. Tinkham, *Introduction to Superconductivity* (Krieger, Malabar, 1975).
- [4] H.J.A. Molegraaf, C. Presura, D. van der Marel, P.H. Kes, M. Li, Science 295, 2239 (2002).
- [5] G. Deutscher, A.F. Santander-Syro, N. Bontemps, Phys. Rev. B 72, 092504 (2005).

- [6] M.M. Doria, S. Salem-Sughi Jr., I.G. de Oliveira, L. Ghivelder, E.H. Brandt, Phys. Rev. B 65, 144509 (2002).
- [7] M.M Doria, J. Supercond. Nov. Magn. 22 (2009) 235.
- [8] M.M Doria, J.E. Gubernatis, D. Rainer, Phys. Rev. B 39, 9573 (1989).
- [9] S. Salem-Sugui Jr., M.M. Doria, A.D. Alvarenga, V.N. Vieira, P.F. Farinas, J.P. Sinnecker, Phys. Rev. B 76, 132502 (2007).
- [10] M.M. Doria and S. Salem-Sugui Jr. Phys. Rev. B 78, 134527 (2008).
- [11] J.A. Osborn, Phys. Rev. 67, 351 (1945).
- [12] F.T. Dias, V.N. Vieira, P. Rodrigues Jr., X. Obradors, P. Pureur and J. Schaf, Phys. Rev. B 77, 134503 (2008).
- [13] P. Rodrigues Jr., J. Schaf and P.Pureur, Phys. Rev. B 49, 15292 (1994).
- [14] J.R.L. de Almeida and D.J. Thouless, J. Phys. A 11, 983 (1978).
- [15] M. Gabay and G. Toulouse, Phys. Rev. Lett. 47, 201 (1981).
- [16] N. de Courtenay, A. Fert and I.A. Campbell, Phys. Rev. B 30, 6791 (1984).
- [17] P.G. de Gennes, *Superconductivity of metals and alloys* (Addison Wesley Publishing Co., 1989)
- [18] Z. Hao, J.R. Clem, Phys. Rev. Lett. 67, 2371 (1991).
- [19] M. Cyrot, D. Pavuna, *Introduction to Superconductivity and high Tc materials* (World Scientific Publications, Co.Pte.Ltd, 1992).
- [20] K.A. Muller, M. Takashige and J.G. Bednorz, Phys. Rev. Lett. 58, 1143 (1987).
- [21] V.N. Vieira and J. Schaf, Phys. Rev. B 65, 144531 (2002).
- [22] H. Kawamura and M.S. Li, J. Phys. Soc. Jpn. 66, 2110 (1997).
- [23] G. Blatter, M.V. Feigel'man, V.B. Geshkenbein, A.I. Larkin and V.M. Vinokur, Rev. Mod. Phys. 66, 1125 (1994).